Published in final edited form as:
Biochemistry. 2011 February 15; 50(6): 1091–1100. doi:10.1021/bi101741v.

Toxoflavin Lyase Requires a Novel 1-His-2-Carboxylate Facial Triad[†,‡]

Michael K. Fenwick[1], **Benjamin Philmus**[⊥], **Tadhg P. Begley**[*,⊥], and **Steven E. Ealick**[1,*]

[1] Department of Chemistry and Chemical Biology, Cornell University, Ithaca, New York 14853

[⊥] Department of Chemistry, Texas A&M University, College Station, TX 77843

Abstract

High resolution crystal structures are reported for apo, holo, and substrate-bound forms of a toxoflavin-degrading metalloenzyme (TflA). In addition, the degradation reaction is shown to be dependent on oxygen, Mn(II), and dithiothreitol *in vitro*. Despite its low sequence identity with proteins of known structure, TflA is structurally homologous to proteins of the vicinal oxygen chelate superfamily. Like other metalloenzymes in this superfamily, the TflA fold contains four modules that associate to form a metal binding site; however, the fold displays a rare rearrangement of the structural modules indicative of domain permutation. Moreover, unlike the 2-His-1-carboxylate facial triad commonly utilized by vicinal oxygen chelate dioxygenases and other dioxygen-activating non-heme Fe(II) enzymes, the metal center in TflA consists of a 1-His-2-carboxylate facial triad. The substrate-bound complex shows square-pyramidal geometry in which one position is occupied by O5 of toxoflavin. The open coordination site is predicted to be the dioxygen binding site. TflA appears to stabilize the reduced form of toxoflavin through second-sphere interactions. This anionic species is predicted to be the electron source responsible for reductive activation of oxygen to produce a peroxytoxoflavin intermediate.

Toxoflavin (Figure 1A) is an azapteridine that is toxic to various plants, fungi, animals, and bacteria. It is synthesized by several bacteria, including *Burkholderia glumae, B. plantarii*, *B. gladioli* pathovar *cocovenenans*, and *Streptomyces* (1, 2). Toxoflavin toxicity is attributed to its ability to act as an effective electron carrier, which allows it to bypass the cytochrome electron transport system and produce hydrogen peroxide in the presence of oxygen (3, 4).

Recently, toxoflavin has gained increasing interest, particularly in the agricultural sciences. Infection of rice plants by toxoflavin-producing bacteria has led to significant losses of rice crops in the United States and Asia (5–8). The identification of toxoflavin as the virulent agent motivated the development of transgenic plants that degrade toxoflavin by expressing the toxoflavin lyase gene (*tflA*) of *Paenibacillus polymyxa* JH2 (9). Unlike their non-transgenic counterparts, these plants were found to grow normally when treated with toxoflavin. *In vitro*, the enzymatic degradation of toxoflavin by TflA was shown to depend

[†]This work was supported by NIH grant GM73220 (S. E. E.) and is based upon research conducted at the Advanced Photon Source on the Northeastern Collaborative Access Team beamlines, which are supported by award RR-15301 from the National Institutes of Health, and at the Cornell High Energy Synchrotron Source (CHESS), which is supported by award RR-01646 from the National Institutes of Health. Use of the Advanced Photon Source is supported by the U.S. Department of Energy, Office of Basic Energy Sciences, under Contract No. DE-AC02-06CH11357. CHESS is supported by the National Science Foundation and the National Institute of General Medical Sciences under NSF award DMR-0225180.

[‡]The Protein Data Bank codes have been deposited under the accession numbers 3PKV, 3PKW, and 3PKX for apo, holo, and toxoflavin-bound TflA, respectively.

[*]To whom correspondence should be addressed at the Department of Chemistry and Chemical Biology, Cornell University, Ithaca, NY 14853. Telephone: (607) 255-7961. Fax: (607) 255-1227. begley@chem.tamu.edu, see3@cornell.edu.

on Mn(II) and the reducing agent dithiothreitol (DTT) (9); however, neither the molecular mechanism underlying the reaction nor the reaction product is known.

Here, we report crystal structures of metal free TflA (apo), TflA-Mn(II) (holo), and the holo-TflA-toxoflavin complex. In addition, we demonstrate biochemically that the conversion of toxoflavin requires molecular oxygen in addition to Mn(II) and a reducing agent (9). The crystal structures show that TflA adopts a structural fold similar to that of vicinal oxygen chelate (VOC) superfamily proteins (10–13) and contains a Mn(II) site. One of the key distinguishing features of TflA is its utilization of a 1-His-2-carboxylate facial triad of Mn(II)-binding ligands characterized by one histidine residue and two monodentate carboxylate groups, similar to the 2-His-1-carboxylate facial triad (14). In the toxoflavin complex, the Mn(II) is also chelated by O5 from toxoflavin and a water molecule, with the open coordination site being the putative dioxygen binding site. Second-sphere interactions provide clues about the tautomeric state and charge of the bound toxoflavin. From this structure and the dependence of the reaction on a reducing agent, a molecular model of a peroxytoxoflavin intermediate was constructed.

MATERIALS AND METHODS

Protein Expression and Purification

The toxoflavin lyase analyzed in this study comprised the 221 residue product of the *tflA* gene from *P. polymyxa* JH2 (9) and the N- and C-terminal poly-histidine tags MGSDKIHHHHHHSSGENLYFQGH and LEHHHHHH, respectively. The native protein was expressed in *Escherichia coli* BL21(DE3) grown in Luria-Bertani media. Typically, cells were grown in baffled shaker flasks at 37 °C until an $OD_{600\ nm}$ of 0.5–0.9 was reached. The flasks were then moved to ice for approximately 1 h, supplemented with isopropyl 1-β-*D*-galactopyranoside to 0.5 mM, and shaken again at 15 °C for a minimum of 18 h. Cell pellets from 1 or 2 L of culture were lysed via sonication on ice and centrifuged twice at 4 °C, 55,000 × g, and for at least 25 min/cycle. The resulting supernatants were subjected to nickel-affinity chromatography and the purity of the protein was verified to be in excess of 95% by sodium dodecyl sulfate poly-acrylamide gel electrophoresis analysis (15). Selenomethionine (SeMet)-substituted TflA was expressed in *E. coli* B834 grown in 4 L of M9 minimal media containing 4 g/L dextrose, 50 mg/L L-SeMet, 40 mg/L of the remaining 19 L-amino acids, 2 mM $MgSO_4$, 0.1 mM $CaCl_2$, 25 mg/L $FeSO_4$, 1× minimal essential medium vitamin solution (Invitrogen) and 40 mg/L kanamycin. These cells were grown and induced as described for the BL21 cultures. SeMet-TflA was purified by nickel-affinity and size exclusion chromatography using buffers supplemented with 1–2 mM DTT. Purified TflA was concentrated to approximately 50 mg/mL based on measurements of light absorbance at 280 nm and an estimated extinction coefficient of 23,000 M^{-1} cm^{-1} (16).

Crystallization and Structure Determination

Crystals were grown using hanging drop vapor diffusion starting with a 1:1 ratio of protein to reservoir solution and equilibrated at 22 °C. For crystallization of the native protein, the reservoir solution consisted of 1.2 M NaH_2PO_4, 0.8 M K_2HPO_4, 0.1 M 3-(cyclohexylamino)-1-propanesulfonic acid (CAPS), pH 10.5, and 0.2 M Li_2SO_4. Crystals of SeMet-TflA grew in drops made from a modified reservoir solution of 1.05 M NaH_2PO_4, 0.86 M K_2HPO_4, 0.091 M CAPS, pH 10.5, 0.14 M Li_2SO_4, and 18 mM DTT.

Prior to cryo-cooling, the crystals of apo-TflA were soaked in a cryoprotectant consisting of a 1:1 ratio of reservoir buffer and a solution of 30% (*v*/*v*) glycerol and 30% (*v*/*v*) ethylene glycol to which $MnCl_2$ was added to a final concentration of 5 mM; however, no density for Mn(II) was observed in the active site for this particular structure. For the TflA-Mn(II)-

toxoflavin complex, crystals were first transferred into drops of stabilizing solution prepared from 3 μL of 25% (*w*/*v*) PEG3000 and 1% (*v*/*v*) reservoir solution, where 0.2 M Li_2SO_4 was replaced with 0.2 M NaCl, final pH 6.4, 0.5 μL of 25 mM $MnCl_2$, and 0.5 μL of 2.5 mM toxoflavin. The toxoflavin concentration was then increased through two 0.5 μL additions of 10 and 100 mM stocks after which time the crystals were allowed to soak for approximately 45 min. Immediately preceding cryo-cooling, 2 μL of 0.2 M DTT followed by 3 μL of 50% (*w*/*v*) PEG3000 were added to these drops and the crystals were picked up and flash cooled without delay. For the holo-TflA structure, a similar procedure was followed but with toxoflavin replaced by the uncharacterized reaction products; however, in the structure electron density was only present for Mn(II) and coordinating waters.

Data Collection and Processing

X-ray diffraction experiments were performed at the Advanced Photon Source (APS) and the Cornell High Energy Synchrotron Source (CHESS). In all cases, the rotation method was employed with an oscillation range of 1.0°/frame and crystals were irradiated at cryogenic temperatures near 100 K. At the APS, the native and SeMet-TflA crystals were exposed to X-rays at the selenium edge for 1.0 s. Images were recorded on an ADSC Q315 CCD detector with a crystal to detector distance of 200 mm. At CHESS, the holo and substrate-bound TflA crystals were exposed to X-rays for 1.5 s. Images were collected using an ADSC Q270 CCD detector with crystal to detector distances of 210 and 190 mm, respectively.

Images were indexed, integrated, scaled, and merged using the program HKL2000 (17). Final sets of merged intensities for the apo, holo, and toxoflavin-bound TflA were derived from 150, 130, and 220 X-ray images and corresponded to 1.34, 1.80, and 1.50 Å resolution, respectively. The final SeMet-TflA data set with unmerged Bijvoet pairs was obtained from 150 images and had a resolution of 1.70 Å. Data collection and processing statistics are summarized in Table 1.

Structure Determination and Refinement

The crystal structure of TflA was determined using single-wavelength anomalous diffraction (SAD) phasing and SeMet-TflA. This crystal belonged to the rhombohedral space group *R*3 and had unit cell dimensions a = 110.9 Å and c = 58.3 Å. The asymmetric unit contained a single copy of the protein and the estimated solvent content of the unit cell was 49.6%. The selenium substructure corresponding to Met17, Met24, and Met203 was obtained using SHELXD (18,19). The AutoSol routine of PHENIX (20) successfully placed residues 2–221 of SeMet-TflA plus Leu222 from the C-terminal tag using the resulting 1.70 Å resolution electron density map. Refinement was carried out using PHENIX and graphical manipulations were performed with COOT (21). The final structural model was refined to R_{work} and R_{free} values of 17.4 and 19.4%, respectively. Refinement statistics are shown in Table 2.

The SeMet-TflA structure was used to provide initial phases for the structures of the apo, holo, and substrate-bound forms of TflA. All crystals belonged to the same space group and had similar unit cell dimensions to the SeMet-TflA crystal. Structure refinements were carried out in two steps. The first consisted of seven cycles of maximum likelihood refinement using PHENIX in which water molecules and side chain rotamers were added or updated automatically, and simulated annealing was performed in the first and fourth cycles. Default parameters were employed throughout. The structures were then examined and modifications to the protein were made where appropriate. For the holo-TflA and TflA-Mn(II)-toxoflavin structures, active site water molecules were removed and Mn(II), or toxoflavin and Mn(II), respectively, were placed into F_o-F_c electron density (Figure 1B).

Toxoflavin was initially built using the electronic ligand builder and optimization workbench in PHENIX (22). Beginning with a dihydro form of toxoflavin with atoms N4 and N8 protonated, the AM1 semi-empirical quantum mechanical method was employed to obtain ligand coordinates and geometry restraints.

In the second step, five additional rounds of maximum likelihood refinement were performed in PHENIX with water molecule updating. The program REDUCE (23) was applied for choosing side chain orientations for asparagine, glutamine, and histidine residues and the structure was subsequently analyzed using COOT and PROCHECK (24). Finally, water molecules with B-factors greater than 50.0 $Å^2$ and a $2F_o$-F_c map σ-level less than 1.0 electrons/$Å^3$ were removed, and all remaining waters were examined individually. Superimposition of native and SeMet-TflA mainchain atoms of the apoenzyme showed a root mean square deviation (RMSD) of 0.12 Å indicating that no significant backbone structural changes arose from selenium substitution of the methionyl sulfur atoms. Refinement statistics are summarized in Table 2.

Molecular Modeling of Peroxytoxoflavin

A molecular model of a peroxytoxoflavin intermediate was constructed based on an assumed reaction of molecular oxygen with carbon C4a of reduced toxoflavin. The model was initially built with an -O-O-H moiety covalently bonded to carbon C4a of toxoflavin. The three dimensional structure was drawn using ChemSketch (ACD Labs) and then optimized *in vacuo* using the AM1 semi-empirical quantum mechanical method within the electronic ligand builder and optimization workbench of PHENIX (22). The optimized structure was placed into the active site of TflA by superimposition onto the experimental toxoflavin structure in the holo-TflA-toxoflavin complex. The terminal hydrogen atom of the -O-O-H moiety was removed and the coordinates of the terminal oxygen atom were altered to give a best fit to octahedral coordination. This was done by calculating the torsional angle that minimized the sum of squares of deviations of the five oxygen-Mn(II)-ligand angles from ideal octahedral angles, assuming a fixed optimized O-O bond distance of 1.32 Å and C4a-O-O angle of 116°.

Toxoflavin Synthesis

Toxoflavin was synthesized as previously described (25).

UV-Vis Spectroscopy

UV-visible spectra were recorded for solutions of toxoflavin containing or lacking DTT. For the former case, toxoflavin, dissolved in 10 mM potassium phosphate buffer (pH 7.0) to a final concentration of 9 mM, was combined with an equal volume of 10 mM DTT dissolved in water. In the absence of DTT, toxoflavin was mixed with an equal volume of water. UV-visible spectra were determined using a NanoDrop 2000 (ThermoScientific).

Oxygen Dependence of TflA

For testing the oxygen dependence of the TflA reaction all the components were allowed to gas exchange in a COY anaerobic chamber operating at less than 1 ppm O_2 for 30–45 min prior to mixing. The aerobic reaction mixtures were removed from the anaerobic chamber and incubated at room temperature for approximately 1 h, which corresponded to the time required for the control reaction mixture lacking TflA, to turn yellow (indicative of toxoflavin re-oxidation) and the reactions heat denatured (95 °C for 5 min) prior to protein removal. The anaerobic reactions were left in the anaerobic chamber for 1h and heat denatured (95 °C for 5 min) prior to exposure to oxygen. The reactions were then passed through PALL life sciences protein concentrators (10,000 MWCO, 14,000 × g, 30 min, and

4 °C). Samples (20 μL) of the flow through volumes were analyzed by HPLC as described below.

TflA Activity Assays

Reaction mixtures consisted of 50 μL solutions of 20 mM Tris (pH 6.5), 10 mM $MnCl_2$, 0.5 mM toxoflavin, and 9 μM TflA and were initiated by the addition of DTT to a final concentration of 10 mM. At the specified time points (1, 5, 10, 15, and 30 min), the reactions were quenched by addition of 100 μL 10 M urea followed by filtration through PALL protein concentrators (10,000 MWCO, 14,000 × g, 30 min, 4 °C). A portion of the reaction mixtures (100 μL) were analyzed via HPLC as described below.

TflA Inactivation Studies

Water (145 μL), 5 μL Tris, (1 M, pH 7.0) and 25 μL TflA (90 μM) were added to a 1.5 mL micro-centrifuge tube. Aliquots (35 μL) were then placed in new micro-centrifuge tubes. To each was added 2 μL water or 2 μL EDTA (20 mM) and the mixtures were incubated for 1 h at room temperature. To each of these mixtures was added 3 μL $MnCl_2$ (0.1 M) or 3 μL water followed by 5 μL toxoflavin (5 mM) and the reaction was initiated by addition of 5 μL DTT (0.1 M). The mixtures were then incubated for 2 h at 30 °C followed by addition of 200 μL 10 M urea. The mixtures were incubated at room temperature for 15–20 min and then filtered through PALL life sciences protein concentrators (10,000 MWCO, 14,000 × g, 30 min, 4 °C) and 100 μL samples of the concentrator flow through were analyzed by HPLC as described below.

HPLC Analysis

HPLC analysis was performed using an Agilent 1200 HPLC system equipped with a quaternary pump and autosampler and monitored with a 1200 DAD detector using a Gemini C6-Phenyl column (4.6 × 150 mm, 5μm, 110 Å, Phenomenex) at a flow rate of 1 mL/min. Line A was water, Line B was 10 mM potassium phosphate (pH 6.8) and Line C was methanol. For the time course assays the following gradient program was used. The column was pre-equilibrated in 100% A prior to sample injection. The composition of the mobile phase was changed to 45% A/55% B over 10 min using a linear gradient followed by changing to 15% A/30% B/55% C over the next 10 min. The mobile phase was held at this composition for 2 min and then recycled to 100% A in 1 min. The column was then equilibrated in 100% A for 7 min prior to the next injection. For all other assays the following gradient was used. The mobile phase was initially 100% A and held for 1 min followed by changing to 50% A/50% C over the next 6 min. The composition was held at 50% A/50% B for 3 min and then recycled to 100% A in 1 min. The column was then equilibrated in 100% A for 7 min prior to the next injection.

Large Scale Purification of the Enzymatic Product

A master mix of 495 μL 50 mM potassium phosphate (pH 6.8), 80 μL toxoflavin (5 mM), 80 μL $MnCl_2$ (0.1 M) and 80 μL TflA (~200 μM) were mixed in a micro-centrifuge tube. The mixture was aliquoted to a total of 4 tubes containing 190 μL master mix, to which 10 μL DTT (0.1 M) was added to initiate the reaction. A total of 14 reactions were performed in this manner. The reactions were incubated at 30 °C for 45 min followed by centrifugation to eliminate solid precipitate (14,000 × g, 15 min, 4 °C) and then filtered through a PALL life sciences protein concentrator (10,000 MWCO, 14,000 × g, 60 min, 4 °C). The product was then purified by HPLC using a SPLC-18DB column (10 × 250 mm, 5 μm, Supelco) at a flow rate of 2 mL/min using an Agilent 100 HPLC system with quaternary pump and manual injector where Line A was water and Line B was methanol. The column was pre-equilibrated in 100% A and upon injection of the sample immediately switched to 95% A/

5% B. This composition was held for 2 min and then changed to 35% A/65% B over the next 18 min using a linear gradient. This composition was held for 5 min then the mobile phase was recycled to 100% A in 1 min and the column was equilibrated in 100% A for 9 min prior to the injection of the next sample. Typical injection volumes were 25–50 μL. The product eluted at approximately 12 min and was collected and fractions pooled. The solvent was removed under evaporation at reduced pressure. The residue was re-dissolved in 450 μL water and 50 μL D_2O and analyzed via NMR spectroscopy. The spectra obtained were insufficient to unambiguously assign a structure to the reaction product.

Figure Preparation

Illustrations were prepared using Chimera (26,27) and ChemDraw (CambridgeSoft).

RESULTS

Structure of TflA

TflA is an α/β protein formed from two domains each containing a seven-stranded mixed β-sheet (Figure 2A). The β-sheet topology of domain 1 is β2↑β3↓β4↑β1↑β12↓β13↑β14↓ whereas that of domain 2 is similar with β6↑β7↓β8↑β5↑β9↓β11↓β10↑ (Figure 2B). Domains 1 and 2 are related by pseudo twofold symmetry and are joined by two crossovers: one joining β4 and β5 and the second joining β11 and β12.

Domain 1 consists of two modules, M_1 and M_4. M_1 contains a βαβββ fold formed by β-strands 1–4 with helix α1 linking strands β1 and β2, and module M_4 contains a βββ fold formed by β-strands 12–14. Similarly, domain 2 also comprises two modules, M_2 and M_3. M_2 contains a βαβββ fold formed by β-strands 5–8 with helix α2 linking β-strands 5 and 6, and M_3 contains a βαββ fold formed by β-strands 9–11 with helix α3 joining β-strands 9 and 10. Modules M_1 and M_2 are structurally similar to each other and are related by pseudo twofold symmetry. Modules M_3 and M_4 are also related by the same pseudo twofold axis.

The mixed β-sheet of domain 2 makes a U-shaped cavity that harbors a metal binding site, whereas that of domain 1 forms a flatter surface that lacks a metal binding site. The two domains pack together with their β-sheets back-to-back such that M_1 packs against M_2 and M_3 packs against M_4. The three α-helices are largely solvent exposed and reside outside the β-sheet core.

TflA Active Site

In the substrate-bound complex, toxoflavin interacts with TflA residues in M_2, M_3, and the loop connecting M_3 and M_4 (Figure 3). Toxoflavin O5 makes a hydrogen bond with the hydroxyl of Tyr103. The triazine ring shows partial π-stacking with the side chain of Phe94. The N1 methyl group and the triazine ring make hydrophobic interactions with Leu170 and Phe172, respectively. The pyrimidine ring makes hydrophobic interactions with the side chains of Leu190 and Trp189 in the loop connecting M_3 and M_4. Toxoflavin O7 and N8 hydrogen bond to the guanidinium group of Arg187, and O7 hydrogen bonds to the backbone nitrogen atom of Leu190. Complex formation also results in a coordinate covalent bond between toxoflavin O5 and Mn(II), and hydrogen bonds between toxoflavin N2 and W4, and between toxoflavin N4 and W3.

Inferred hydrogen bonds between N2, N4, and N8 and side chains of TflA suggest a toxoflavin protonation state compatible with the reduced form, which is required for catalysis. Toxoflavin O7 and N8 accept hydrogen bonds from Arg187 suggesting N8 is not protonated. W3 donates hydrogen bonds to Glu113 and Glu138 (both metal ligands) suggesting that it accepts a hydrogen bond from toxoflavin N4 (2.9 Å). The local atomic

geometry around toxoflavin N2 is less informative. The N2-W4 distance is 3.1 Å; however, if N2 were protonated the N2-H…W4 angle would be 117°, suggesting that N2 is not likely to act a strong hydrogen bond donor.

Mn(II) Binding Site

The metal binding site consists of a facial triad comprising residues His60, Glu113, and Glu138 (1-His-2-carboxylate). His60 and Glu113 are located in β5 and β8, respectively, and Glu138 resides in β9. The side chains of these residues extend into the active site cavity to supply three *cis*-ligands for Mn(II), leaving three open coordination sites for other ligands.

In the apoenzyme, nitrogen Nε2 of His60 forms a hydrogen bond with one of the carboxylate oxygen atoms of Glu138 (Figure 4A). Water molecules W1, W3, and W6 occupy positions opposite the facial triad in the unoccupied Mn(II) binding site. Water molecule W1 hydrogen bonds to the hydroxyl of Tyr103. The electron density for water molecules W3 and W6 is less distinct than W1 and the hydrogen bonding interactions are probably dynamic.

In the holoenzyme, the three open coordination sites are occupied by water molecules, which all have well-defined electron density. The overall arrangement of the coordination sphere is octahedral (Figure 4B), with all of the 15 ligand-Mn(II)-ligand angles being within 15° of ideal octahedral angles. None of the water molecule-Mn(II) distances suggest hydroxide character. Rather, all of the water molecules (W1, W2, and W3) are separated from Mn(II) by at least 2.2 Å, which is consistent with overall neutrality for the metal center. Water molecules W1 and W3 make hydrogen bonds with second-sphere water molecules and protein ligands. W1 hydrogen bonds to the hydroxyl of Tyr103 and W3 hydrogen bonds to the carboxylates of Glu113 and Glu138. On the other hand, W2 hydrogen bonds to two other water molecules, but no protein atoms. These waters are involved in an elaborate hydrogen bonding network that is disrupted when toxoflavin binds.

Finally, the structure of the holo-TflA-toxoflavin complex shows a metal center having square pyramidal geometry (Figure 4C). Ligands are provided by Nε2 of His60, W3, O5 of toxoflavin and the carboxylates of Glu113 and Glu138. The vacant coordination site is *trans* to the carboxylate of Glu113 and corresponds to the position occupied by W2 in the holoenzyme. Toxoflavin O5 is located at the site occupied by W1 in the apo- and holoenzymes and is the only toxoflavin atom that chelates Mn(II). W3 occupies the same position in both the holoenzyme and holo-TflA-toxoflavin complex and appears to be neutral based on its distance of 2.2 Å from Mn(II).

Model of Peroxytoxoflavin Bound to TflA

A model of peroxytoxoflavin in the active site of TflA is shown in Figure 5. Covalent addition of molecular oxygen to carbon C4a of reduced toxoflavin is predicted to result in tetrahedral geometry at this position. Construction of a peroxytoxoflavin-TflA molecular model shows that the tetrahedral geometry can be achieved while maintaining an octahedral coordination sphere. All five of the resulting oxygen-Mn(II)-ligand angles are within 13.0° of the ideal octahedral angles. The resulting O-O-Mn(II) angle is 128.8° and the separation distance between Mn and the distal peroxy oxygen atom is 2.2 Å. This geometry results in a bent ligand structure near the peroxy moiety. The opposite side of the ligand near carbon C8a is also slightly bent but its local geometry results in a higher degree of planarity. All of the key interactions observed in the holo-TflA-toxoflavin complex are also present in the structure of the putative peroxytoxoflavin intermediate without significant change in the associated interatomic distances.

Biochemical Analysis of TflA

Initial attempts to reconstitute the *in vitro* activity of TflA were made by premixing toxoflavin, Mn(II), and DTT and the reaction was initiated by the addition of TflA. These initial attempts resulted in extremely low amounts of the toxoflavin degradation product being formed. Upon closer inspection it was noticed that prior to TflA addition the addition of DTT caused the characteristic yellow color of toxoflavin to disappear. UV-Vis spectroscopic investigations revealed a marked spectral shift when toxoflavin and DTT were mixed in the absence of TflA (Figure 6A). The reaction product was unstable and rapidly re-oxidized to toxoflavin in the presence of oxygen (Figure 6A). This is similar to the findings of Latuasan and Berends and their investigations with yeast cell free lysate and NADPH (3). These results led to the hypothesis that the reduced form of toxoflavin was the species bound to and acted upon by TflA. Therefore all assays were initiated by the addition of DTT rather than enzyme because of the rapidity of the re-oxidation of toxoflavin.

Initial studies of TflA activity revealed that a single product was formed as determined via HPLC and its formation was TflA, Mn(II), and DTT dependent (Figure 6B). Other reductants, such as NADH and sodium dithionite, also resulted in product formation although the conversion was not as high as seen with DTT.

Treatment of TflA with EDTA abolished catalytic activity suggesting that the reaction requires a metal. Addition of metal ions to the apoenzyme resulted in high activity for Mn(II), revealed very low activity for Fe(II), and no activity for Fe(III), Cu(I), Cu(II), Co(II), and Ba(II). The requirement for oxygen was also investigated since BLAST analysis revealed weak homology to dioxygenases. Assembly of the reaction in an anaerobic environment followed by incubation either anaerobically or aerobically demonstrated that oxygen was essential for product formation. In addition the presence of hydrogen peroxide did not afford product when DTT was omitted from the reaction mixture (data not shown) suggesting that either the peroxytoxoflavin intermediate is essential for catalysis or that the oxidized form of toxoflavin is unable to bind to the active site of TflA.

DISCUSSION

Similarity of TflA to Other Proteins

Alignment of the structure of TflA against structures in the Protein Data Bank (PDB) (28) using the DALI server (29) indicates that TflA is structurally homologous to several proteins. Hypothetical proteins 1ZSW and 3OAJ have the highest Z-scores of 12.1 and 11.5, respectively. The structural alignments include approximately 80% of the TflA residues and show sequence identities with TflA of 11 and 14%, respectively. These two homologs contain two α/β domains that are each composed of an eight-stranded β-sheet with α-helices near the first and last β-strand. Similar to TflA, the two domains are related by pseudo twofold symmetry and are constructed from similar βαββ modules. However, only two subdomains of TflA contain complete βαββ modules (M_1 and M_2), whereas these homologs contain four complete βαββ modules. Furthermore, whereas TflA has a metal binding site located between subdomains M_2 and M_3, these homologs have a metal binding site between subdomains M_1 and M_4.

Many of the remaining structural homologs identified by the DALI search are members of the VOC superfamily and have known functions. These homologs include glyoxalases (PDB IDs 1FRO and 1FA5) (30,31), methylmalonyl-CoA epimerases (PDB ID 1JC5) (32), fosfomycin resistance proteins (PDB ID 1LQP) (33), extradiol (PDB IDs 1HAN, 1MPY, 1DHY, and 1F1U) (34–37) and α-keto acid-dependent dioxygenases (PDB IDs 1T47 and 1CJX) (38,39), and non-enzymatic bleomycin-resistance proteins (PDB ID 1BYL) (40). These homologs have DALI Z-scores between 5.0 and 9.0 and display diverse sequences

with less than 20% identity compared to TflA. Like TflA, these proteins form structures of two domains, which contain mixed β-sheets built primarily from βαββ-like modules. The extradiol and a-keto acid-dependent dioxygenases form such structures via a single polypeptide chain comprising four tandem βαββ-like modules, similar to proteins 1ZSW and 3OAJ. In contrast, the glyoxalases, methylmalonyl-CoA epimerases, and fosfomycin- and bleomycin-resistance proteins are homodimers with each protomer containing tandem βαββ-like modules.

Despite the low sequence identity between TflA and its structural homologs, the primary structure of TflA contains well-defined signature sequences of the βαββ modules of VOC superfamily proteins (12). For M_1 and M_3 of structures containing four βαββ modules, the signature sequence is $S_{1,3}$ = $DX_6FXTX_2LG(F,M,L)X_6D$ and occurs near the single α-helix. For modules M_2 and M_4, $S_{2,4}$ = $(D,T)PXGX_2(L,V,I)(E,H)$ occurs near the $\beta_3\beta_4$ fragment. LG(F,M,L) in $S_{1,3}$ and PXG in $S_{2,4}$ have also been shown to be highly conserved (12). The stretch of residues Glu13 to Asp35 in M_1 of TflA, specifically ELDRMLAFYTNMLGAQHVHEQAD, is homologous to $S_{1,3}$, with LG being located at the C-terminal end of the α-helix. Furthermore, DPSGNIIE (106–113), which resides in and between β_3 and β_4 of M_2, is equivalent to $S_{2,4}$. Structurally, LG(F,M,L) acts as a helix termination sequence and PXG a turn sequence. In TflA, Leu25-Gly26-Ala27 terminates the α-helix in M_2. Asp106-Pro107-Ser108-Gly109 forms a type-1 β-turn. The signature sequences are not found in modules M_3 and M_4.

Domain Structure of TflA

Studies on the evolution of the VOC superfamily suggest that members derive from a homodimeric ancestor in which each monomer contains two modules (10–13). Each of the two identical metal binding sites of the ancestral enzymes (represented by glyoxalase I, PDB ID 1F9Z) (31) utilizes residues from both subdomains through domain swapping (Figure 7A). The VOC superfamily members containing four modules likely evolved by gene duplication and fusion of the two-module proteins (12). The fused proteins typically have retained only one metal binding site.

Three distinct arrangements of four module proteins have been observed. One domain of TflA is formed from M_1 and M_4 and a second domain is formed from M_2 and M_3 (Figure 7B). The Mn(II) binding site of TflA is located between modules M_2 and M_3 and there are two interdomain crossovers. *Bacillus subtilis* MhqO, (PDB ID 3OAJ) a putative ring-cleaving dioxygenase, shows a modular arrangement similar to that of TflA (Figure 7C); however, the metal binding site is located between modules M_1 and M_4. The VOC superfamily enzymes, represented by 4-hydroxyphenylpyruvate dioxygenase (HPPD) (PDB ID 1CJX) (39) displays a different modular arrangement in which M_1 and M_2 form one domain and M_3 and M_4 form another (Figure 7D). The diversity of domain arrangements and metal binding sites suggests multiple evolutionary paths involving gene fusion, domain swapping (41), circular permutation (42, 43) and individual amino acid mutations.

Comparison with the 2-His-1-carboxylate Facial Triad

The 2-His-1-carboxylate facial triad is a common structural motif found in mononuclear non-heme Fe(II) enzymes that activate molecular oxygen (14,44,45). As its name implies, the metal binding protein ligands occupy a face of an octahedral coordination sphere. However, metal chelation by the triad carboxylate can be mono or bidentate depending on the enzyme. Thus, up to three exogenous ligands can bind to the metal center, making the facial triad a versatile motif for mediating a wide range of chemical transformations. Accordingly, the 2-His-1-carboxylate facial triad is found in a variety of enzymes, including

the VOC superfamily extradiol and a-keto acid-dependent dioxygenases that are structurally homologous to TflA (46).

TflA shows a variation of the 2-His-1-carboxylate facial triad. In this case, a histidine residue is replaced by one glutamate residue, resulting in a 1-His-2-carboxylate facial triad that thus far is observed only in TflA. Figure 8 shows the 2-His-1-carboxylate facial triad of Fe(II)-dependent 2,3-dihydroxybiphenyl 1,2-dioxygenase (DHBD) (34–37) superimposed on the 1-His-2-carboxylate facial triad of Mn(II)-dependent TflA. The metal-binding ligands display similar spatial arrangements but are located in different structural modules. The metal-ligand distances in the two structures are similar; the largest deviation is seen for Glu260 of DHBD, whose metal separation distance is about 0.2 Å shorter than that of Glu113 in TflA. In the absence of substrate, the facial triad of TflA binds to three water molecules with octahedral geometry. In contrast, the facial triad of DHBD binds to two water molecules in a square-pyramidal arrangement.

Mechanistic Implications

TflA is a member of the VOC superfamily and shows structural similarities to dioxygenases. TflA requires oxygen, a reducing agent, and Mn(II), which is chelated by a novel 1-His-2-carboxylate facial triad. These observations suggest that degradation of toxoflavin requires the reduced form of toxoflavin and occurs through a peroxytoxoflavin-TflA intermediate. Modeling studies show that the active site can accommodate such an intermediate while maintaining energetically feasible geometry.

The reduced form of toxoflavin inferred from the structure may be negatively charged since N4 is likely protonated and N8 deprotonated. Based on the chemical structure of toxoflavin and the interaction of toxoflavin with TflA, this putative charge presumably resides partially on O7 and N8 and is stabilized through a salt-bridge with the guanidinium group of Arg187 and through the hydrogen bond between O7 and the backbone amide nitrogen of Leu190. The protonation of N4 appears to be stabilized through hydrogen bonding with water W3, which is oriented to accept a hydrogen bond due to the hydrogen bonds it donates to the two metal-binding carboxylates. The predicted negative charge on toxoflavin is expected to enhance the reductive activation of O_2 to give the peroxytoxoflavin intermediate.

Dioxygen activating non-heme Fe(II) enzymes commonly display pentadentate coordination of Fe(II) after substrate or cofactor binding (46). Thus, this binding step primes the metal center for coordination by dioxygen. In the extradiol dioxygenases of the VOC superfamily, this is achieved through metal coordination by catecholic hydroxyls on the substrate, one of which is deprotonated (37,47). In the a-keto acid-dependent enzymes of the VOC superfamily, this is achieved through metal binding by the a-keto acid in a bidentate fashion utilizing the keto and carboxylate oxygens (48). Similarly, toxoflavin binding to Mn(II) in TflA leads to pentadentate coordination with the open site anticipated to be the dioxygen binding site. However, unlike the dioxygenases, only one atom of the substrate (toxoflavin O5) chelates Mn(II); the other site is occupied by water W3. In addition, Mn(II) does not appear to be chelated by an anionic group, which is likely related to the neutrality of the combination of Mn(II) and the 1-His-2-carboxylate ligands. Finally, the pentadentate metal center does not involve coordination by vicinal oxygens on the substrate.

Due to the paucity of characteristic NMR features, the product of the TflA-catalyzed reaction has not yet been determined. The structure of the enzyme toxoflavin complex however suggests a mechanism for the early events in toxoflavin oxidation that provides a framework for considering possible reaction products. In this mechanism (Figure 9), toxoflavin is reduced by DTT to give dihydrotoxoflavin. This reduction is non-enzymatic and reversible. We suggest structure **2** for the reduction product by analogy to the structure

of dihydroflavin (49). This then binds to the enzyme and is oxidized to hydroperoxide **4**. Analogous chemistry is found in the oxidation of dihydroflavin to give the well-characterized flavin hydroperoxide (49). We envision three possibilities for the next step. Cleavage of the O-O bond would give **5**, which could then undergo rearrangement of the hydroxytoxoflavin, as previously seen for hydroxyflavin (50), and oxidized guanosine (51) followed by further oxidation by the manganese(IV) oxo. Aspects of this chemistry have precedent in the mechanism of the). biopterin-dependent phenylalanine hydroxylase (52 Alternatively, elimination of hydroperoxide, a reaction frequently seen in the aerobic oxidation of dihydroflavin (49), would give **6**, which could undergo further peroxide mediated oxidation or ring A opening reactions (53). The third possibility involves the ring expansion via a Baeyer-53 Villiger reaction producing **7** and Mn(II)-OH. Product identification is essential to differentiate between these possibilities. This is being pursued using a comprehensive set of ^{13}C and ^{15}N-labeled toxoflavin isotopologues, which will facilitate unambiguous NMR characterization.

Acknowledgments

We thank the staff of NE-CAT at the Advanced Photon Source and the staff of the Cornell High Energy Synchrotron Source for assistance with data collection, Dr. Cynthia Kinsland for cloning and purifying initial samples of native TflA and Leslie Kinsland for help in preparing the manuscript.

ABBREVIATIONS

TflA	Toxoflavin lyase
DTT	dithiothreitol
VOC	vicinal oxygen chelate
SeMet	selenomethionine
PDB	Protein Data Bank
PEG	polyethylene glycol
SAD	single-wavelength anomalous dispersion
CAPS	3-(cyclohexylamino)-1-propanesulfonic acid
RMSD	root mean square deviation
DHBD	2,3-dihydroxybiphenyl 1,2-dioxygenase
HPPD	4-hydroxyphenylpyruvate dioxygenase,

References

1. Levenberg B, Linton SN. On the biosynthesis of toxoflavin, an azapteridine antibiotic produced by Pseudomonas cocovenenans. J Biol Chem 1966;241:846–852. [PubMed: 5905124]
2. Lynch, KH.; Dennis, JJ. Burkholderia. In: Liu, D., editor. Molecular detection of foodborne pathogens. CRC Press Taylor and Francis Group; Boca Raton: 2010. p. 331-343.
3. Latuasan HE, Berends W. On the origin of the toxicity of toxoflavin. Biochim Biophys Acta 1961;52:502–508. [PubMed: 14462713]
4. Stern KG. Oxidation-reduction potentials of toxoflavin. Biochem J 1935;29:500–508. [PubMed: 16745691]
5. Goto K, Ohata K. New bacterial diseases of rice (brown stripe and grain rot). Ann Phytopathol Soc Jap 1956;21:46–47.

6. Jeong Y, Kim J, Kim S, Kang Y, Nagamatsu T, Hwang I. Toxoflavin produced by *Burkholderia glumae* causing rice grain rot is responsible for inducing bacterial wilt in many field crops. Plant Disease 2003;87:890–895.
7. Nandakumar R, Shahjahan AKM, Yuan XL, Dickstein ER, Groth DE, Clark CA, Cartwright RD, Rush MC. *Burkholderia glumae* and *B. gladioli* cause bacterial panicle blight in rice in the southern United States. Plant Disease 2009;93:896–905.
8. Uematsu T, Yoshimura D, Nishiyama K, Ibaraki T, Fujii H. Pathogenic bacterium causing seedling rot of rice. Ann Phytopathol Soc Jap 1976;42:464–471.
9. Hwang, IG.; Moon, JS.; Jwa, NS. Organization, W. I. P. TflA gene which can degrade toxoflavin and its chemical derivatives and transgenic organisms expressing TflA gene. 2009.
10. Armstrong RN. Mechanistic diversity in a metalloenzyme superfamily. Biochemistry 2000;39:13625–13632. [PubMed: 11076500]
11. Babbitt PC, Gerlt JA. Understanding enzyme superfamilies. Chemistry as the fundamental determinant in the evolution of new catalytic activities. J Biol Chem 1997;272:30591–30594. [PubMed: 9388188]
12. Bergdoll M, Eltis LD, Cameron AD, Dumas P, Bolin JT. All in the family: structural and evolutionary relationships among three modular proteins with diverse functions and variable assembly. Protein Sci 1998;7:1661–1670. [PubMed: 10082363]
13. Gerlt JA, Babbitt PC. Divergent evolution of enzymatic function: mechanistically diverse superfamilies and functionally distinct suprafamilies. Annu Rev Biochem 2001;70:209–246. [PubMed: 11395407]
14. Que L Jr. One motif--many different reactions. Nat Struct Biol 2000;7:182–184. [PubMed: 10700270]
15. Laemmli UK. Cleavage of structural proteins during the assembly of the head of bacteriaphage T4. Nature 1970;227:680–685. [PubMed: 5432063]
16. Pace CN, Vajdos F, Fee L, Grimsley G, Gray T. How to Measure and Predict the Molar Absorption-Coefficient of a Protein. Protein Sci 1995;4:2411–2423. [PubMed: 8563639]
17. Otwinowski, Z.; Minor, W. Processing of X-ray diffraction data collected in oscillation mode. In: Carter, JCW.; Sweet, RM., editors. Methods Enzymol. Academic Press; New York: 1997. p. 307-326.
18. Schneider TR, Sheldrick GM. Substructure solution with SHELXD. Acta Crystallogr D 2002;58:1772–1779. [PubMed: 12351820]
19. Sheldrick GM. A short history of SHELX. Acta Crystallogr 2008;A A64:112–122.
20. Adams PD, Afonine PV, Bunkóczi G, Chen VB, Davis IW, Echols N, Headd JJ, Hung L-W, Kapral GJ, Grosse-Kunstleve RW, McCoy AJ, Moriarty NW, Oeffner R, Read RJ, Richardson DC, Richardson JS, Terwilliger TC, Zwart PH. PHENIX: a comprehensive Python-based system for macromolecular structure solution. Acta Crystallogr 2010;D D66:213–221.
21. Emsely P, Lohkamp B, Scott WG, Cowtan K. Features and development of Coot. Acta Crystallogr D 2010;66:486–501. [PubMed: 20383002]
22. Moriarty NW, Grosse-Kunstleve RW, Adams PD. electronic Ligand Builder and Optimization Workbench (eLBOW): a tool for ligand coordinate and restraint generation. Acta Crystallogr D 2009;65:1074–1080. [PubMed: 19770504]
23. Word JM, Lovell SC, Richardson JS, Richardson DC. Asparagine and glutamine: using hydrogen atom contacts in the choice of side-chain amide orientation. J Mol Biol 1999;285:1735–1747. [PubMed: 9917408]
24. Laskowski RA, MacArthur MW, Moss DS, Thornton JM. PROCHECK: a program to check the stereochemical quality of protein structures. J Appl Cryst 1993;26:283–291.
25. Black TH. An improved, large-scale synthesis of xanthothricin and reumycin. J Heterocycl Chem 1987;24:1373–1375.
26. Goddard TD, Huang CC, Ferrin TE. Visualizing density maps with UCSF Chimera. J Struct Biol 2007;157:281–287. [PubMed: 16963278]
27. Pettersen EF, Goddard TD, Huang CC, Couch GS, Greenblatt DM, Meng EC, Ferrin TE. UCSF Chimera--a visualization system for exploratory research and analysis. J Comput Chem 2004;25:1605–1612. [PubMed: 15264254]

28. Berman HM, Battistuz T, Bhat TN, Bluhm WF, Bourne PE, Burkhardt K, Feng Z, Gilliland GL, Iype L, Jain S, Fagan P, Marvin J, Padilla D, Ravichandran V, Schneider B, Thanki N, Weissig H, Westbrook JD, Zardecki C. The Protein Data Bank. Acta Crystallogr D 2002;58:899–907. [PubMed: 12037327]
29. Holm L, Rosenstrom P. Dali server: conservation mapping in 3D. Nucleic Acids Res 2010;38(Suppl):W545–549. [PubMed: 20457744]
30. Cameron AD, Olin B, Ridderstrom M, Mannervik B, Jones TA. Crystal structure of human glyoxalase I--evidence for gene duplication and 3D domain swapping. EMBO J 1997;16:3386–3395. [PubMed: 9218781]
31. He MM, Clugston SL, Honek JF, Matthews BW. Determination of the structure of *Escherichia coli* glyoxalase I suggests a structural basis for differential metal activation. Biochemistry 2000;39:8719–8727. [PubMed: 10913283]
32. McCarthy AA, Baker HM, Shewry SC, Patchett ML, Baker EN. Crystal structure of methylmalonyl-coenzyme A epimerase from *P. shermanii*: a novel enzymatic function on an ancient metal binding scaffold. Structure 2001;9:637–646. [PubMed: 11470438]
33. Rife CL, Pharris RE, Newcomer ME, Armstrong RN. Crystal structure of a genomically encoded fosfomycin resistance protein (FosA) at 1.19 Å resolution by MAD phasing off the L-III edge of Tl^{+} J Am Chem Soc 2002;124:11001–11003. [PubMed: 12224946]
34. Han S, Eltis LD, Timmis KN, Muchmore SW, Bolin JT. Crystal structure of the biphenyl-cleaving extradiol dioxygenase from a PCB-degrading pseudomonad. Science 1995;270:976–980. [PubMed: 7481800]
35. Kita A, Kita S, Fujisawa I, Inaka K, Ishida T, Horiike K, Nozaki M, Miki K. An archetypical extradiol-cleaving catecholic dioxygenase: the crystal structure of catechol 2,3-dioxygenase (metapyrocatechase) from *Pseudomonas putida* mt-2. Structure 1999;7:25–34. [PubMed: 10368270]
36. Senda T, Sugiyama K, Narita H, Yamamoto T, Kimbara K, Fukuda M, Sato M, Yano K, Mitsui Y. Three-dimensional structures of free form and two substrate complexes of an extradiol ring-cleavage type dioxygenase, the BphC enzyme from *Pseudomonas* sp. strain KKS102. J Mol Biol 1996;255:735–752. [PubMed: 8636975]
37. Vetting MW, Wackett LP, Que L Jr, Lipscomb JD, Ohlendorf DH. Crystallographic comparison of manganese- and iron-dependent homoprotocatechuate 2,3-dioxygenases. J Bacteriol 2004;186:1945–1958. [PubMed: 15028678]
38. Brownlee JM, Johnson-Winters K, Harrison DH, Moran GR. Structure of the ferrous form of (4-hydroxyphenyl)pyruvate dioxygenase from *Streptomyces avermitilis* in complex with the therapeutic herbicide, NTBC. Biochemistry 2004;43:6370–6377. [PubMed: 15157070]
39. Serre L, Sailland A, Sy D, Boudec P, Rolland A, Pebay-Peyroula E, Cohen-Addad C. Crystal structure of *Pseudomonas fluorescens* 4-hydroxyphenylpyruvate dioxygenase: an enzyme involved in the tyrosine degradation pathway. Structure 1999;7:977–988. [PubMed: 10467142]
40. Dumas P, Bergdoll M, Cagnon C, Masson JM. Crystal structure and site-directed mutagenesis of a bleomycin resistance protein and their significance for drug sequestering. EMBO J 1994;13:2483–2492. [PubMed: 7516875]
41. Saint-Jean AP, Phillips KR, Creighton DJ, Stone MJ. Active monomeric and dimeric forms of *Pseudomonas putida* glyoxalase I: evidence for 3D domain swapping. Biochemistry 1998;37:10345–10353. [PubMed: 9671502]
42. Cunningham BA, Hemperly JJ, Hopp TP, Edelman GM. Favin versus concanavalin A: Circularly permuted amino acid sequences. Proc Natl Acad Sci U S A 1979;76:3218–3222. [PubMed: 16592676]
43. Lindqvist Y, Schneider G. Circular permutations of natural protein sequences: structural evidence. Curr Opin Struct Biol 1997;7:422–427. [PubMed: 9204286]
44. Gerlt JA, Babbitt PC. Mechanistically diverse enzyme superfamilies: the importance of chemistry in the evolution of catalysis. Curr Opin Chem Biol 1998;2:607–612. [PubMed: 9818186]
45. Laughlin LT, Bernat BA, Armstrong RN. Mechanistic imperative for the evolution of a metalloglutathione transferase of the vicinal oxygen chelate superfamily. Chem Biol Interact 1998;111–112:41–50.

46. Koehntop KD, Emerson JP, Que L Jr. The 2-His-1-carboxylate facial triad: a versatile platform for dioxygen activation by mononuclear non-heme iron(II) enzymes. J Biol Inorg Chem 2005;10:87–93. [PubMed: 15739104]
47. Vaillancourt FH, Bolin JT, Eltis LD. The ins and outs of ring-cleaving dioxygenases. Crit Rev Biochem Mol Biol 2006;41:241–267. [PubMed: 16849108]
48. He P, Moran GR. We two alone will sing: the two-substrate a-keto acid-dependent oxygenases. Curr Opin Chem Biol 2009;13:443–450. [PubMed: 19625206]
49. Fagan, RL.; Palfey, BA. Flavin-Dependent Enzymes. In: Lew, M.; Hung-Wen, L., editors. Comprehensive Natural Products II. Elsevier; Oxford: 2010. p. 37-113.
50. Iwata M, Bruice TC, Carrell HL, Glusker JP. Reactions of 4a-peroxides and 4a-pseudobases of N^{10}- and N^{5}-phenethylflavins. J Am Chem Soc 1980;102:5036–5044.
51. Ye Y, Muller JG, Luo W, Mayne CL, Shallop AJ, Jones RA, Burrows CJ. Formation of ^{13}C-, ^{15}N-, and ^{18}O-Labeled Guanidinohydantoin from Guanosine Oxidation with Singlet Oxygen. Implications for Structure and Mechanism. J Am Chem Soc 2003;125:13926–13927. [PubMed: 14611206]
52. Bassan A, Blomberg MRA, Siegbahn PEM. Mechanism of dioxygen cleavage in tetrahydrobiopterin-dependent amino acid hydroxylases. Chem--Eur J 2003;9:106–115.
53. Mukherjee T, Zhang Y, Abdelwahed S, Ealick SE, Begley TP. Catalysis of a Flavoenzyme-Mediated Amide Hydrolysis. J Am Chem Soc 2010;132:1550–1551.
54. Kabsch W, Sander C. Dictionary of protein secondary structure: pattern recognition of hydrogen-bonded and geometrical features. Biopolymers 1983;22:2577–2637. [PubMed: 6667333]

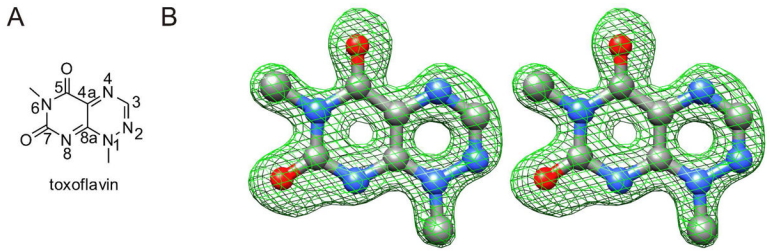

Figure 1.

Structure of toxoflavin. (A) Structural formula and numbering for toxoflavin. (B) F_o-F_c electron density map for toxoflavin. The map is contoured at 3σ. The map was generated using the structure factors for the complex and the refined model of the complex with toxoflavin omitted.

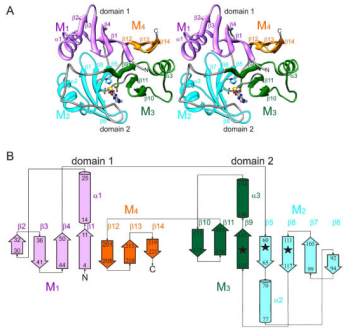

Figure 2.

Structure of TflA. (A) Ribbon representation of the crystal structure of TflA complexed with Mn(II) (yellow sphere) and toxoflavin (ball and sticks). The side chains of facial triad residues His60, Glu113, and Glu138 are depicted as sticks and a metal-chelating water is displayed as a single red sphere. Ribbons and carbon atoms of residues belonging to the modules M_1, M_2, M_3, and M_4 are colored purple, cyan, green and orange, respectively. (B) Secondary structure topology of TflA using the same coloring scheme as in (A). α-helices (cylinders) and β-strands (thick arrows) were assigned using the program DSSP (54). The locations of the facial triad residues are marked with black stars.

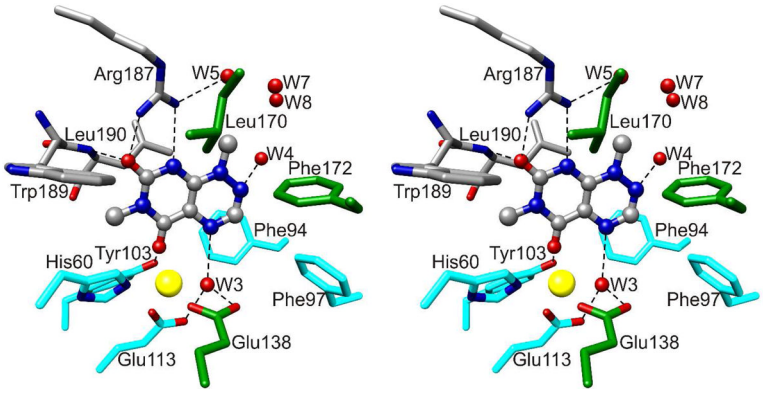

Figure 3.

Stereo diagram of the TflA active site. Active site sidechains of TflA are depicted as sticks with the carbon atoms of residues in M_2, M_3, and the loop connecting M_3 and M_4 colored cyan, green, and gray, respectively. Toxoflavin is shown in ball and stick representation. Mn(II) is represented as a yellow sphere and waters are shown as red spheres.

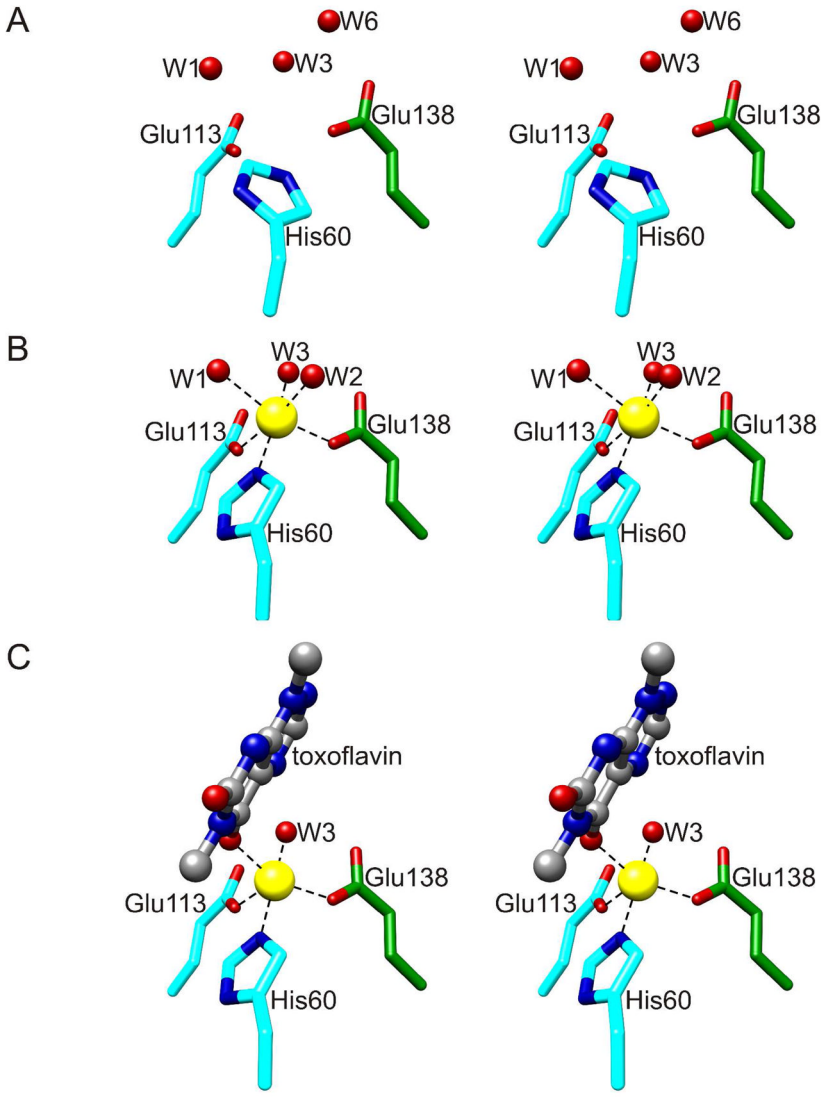

Figure 4.
TflA metal binding site. (A) apo TflA. (B) holo TflA. (C) TflA-toxoflavin-Mn(II) complex. Atoms are represented as in Figure 3.

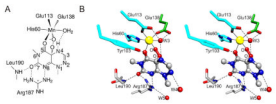

Figure 5.
Structure of a proposed peroxytoxoflavin intermediate. (A) Schematic of the peroxytoxoflavin intermediate showing key interactions with active site residues. (B) Stereodiagram of the molecular model. Atoms are color coded as in Figure 3.

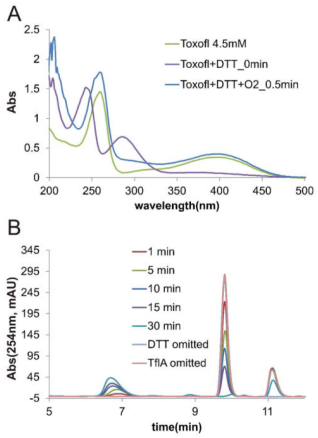

Figure 6.

In vitro assays. (A) UV-visible spectra of toxoflavin (4.5 mM, green trace); toxoflavin (4.5 mM) plus DTT (5 mM), immediately following mixing (purple trace); and toxoflavin (4.5 mM) plus DTT (5 mM), following exposure to air for 30 s (blue trace). (B) Time course for the toxoflavin lyase catalyzed reaction. The product elutes at 6.7 min while toxoflavin elutes at 9.9 min. Spectra were recorded on a Nanodrop 2000 using a volume of 1 μL.

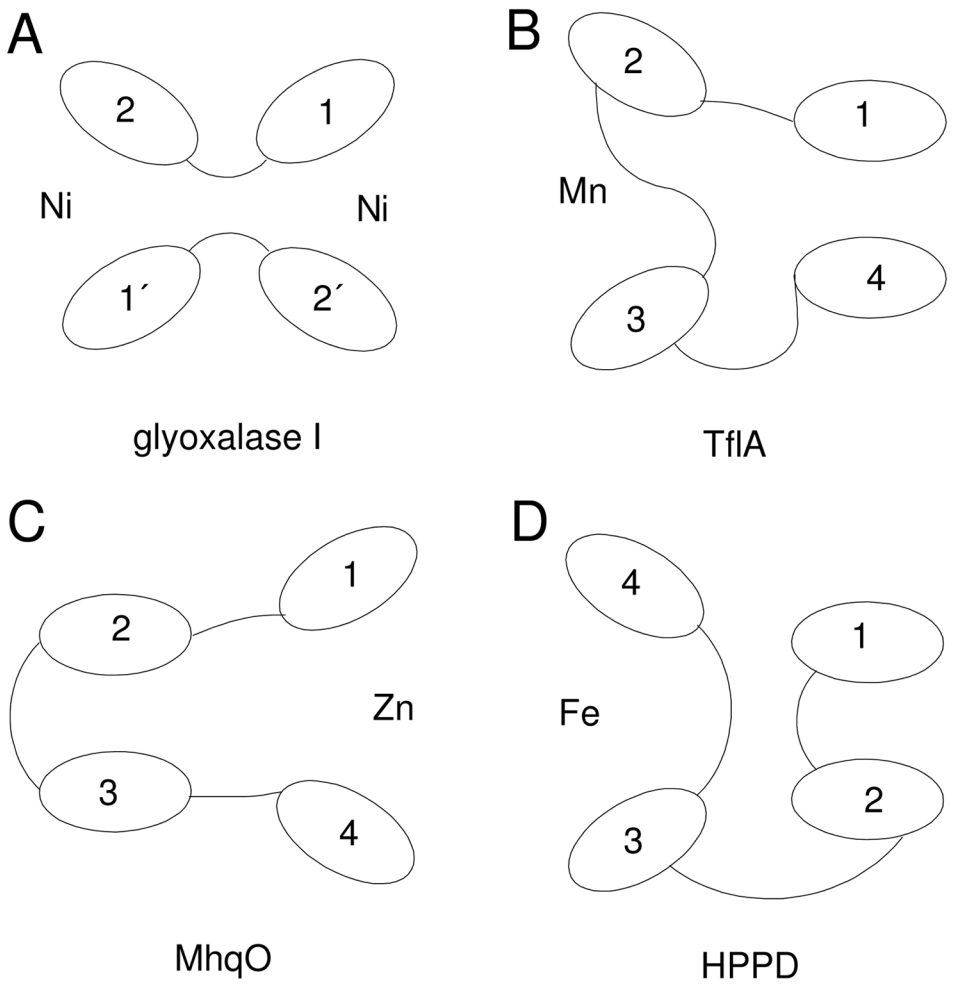

Figure 7.

Modular arrangements in enzymes containing βαβββ folds. (A) Homodimeric family containing modules $M_1$and M_2 and two metal binding sites, represented by glyoxalase I (PDB ID 1F9Z). (B) Four module arrangement in TflA. (C) Four module arrangement in MhqO (PDB ID 3OAJ). (D) Four module arrangement in HPPD (PDB ID 1CJX).

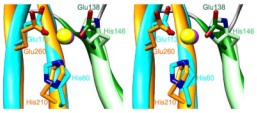

Figure 8.

Comparison of 1-His-2-carboxylate and 2-His-1-carboxylate facial triads. A stereodiagram is shown for the superimposition of the backbone atoms of the three metal-binding ligands of TflA onto the equivalent atoms in DHBD. The yellow sphere represents Mn(II) bound by TflA and the purple sphere signifies Fe(II) bound by DHBD. Coordinating waters and ligands are not shown. The carbon backbone and ribbon representation of residues in M_2, M_3, and M_4 are colored cyan, green (or light green for DHBD), and orange, respectively.

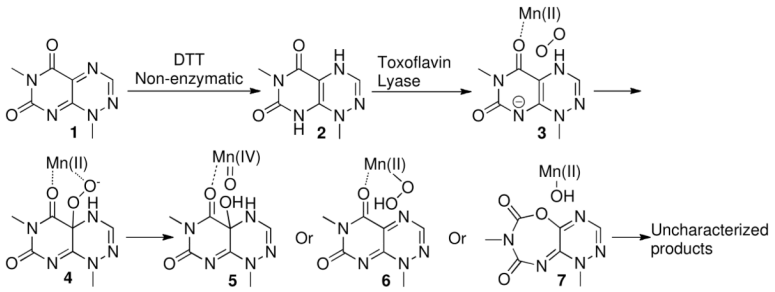

Figure 9.
Mechanistic proposal for the early steps in the toxoflavin lyase mediated toxoflavin oxidation.

TABLE 1

X-ray Data Collection Statistics.

	SeMet-TflA	apo-TflA	holo-TflA	TflA-Tox-Mn
beamline	APS 24-ID-C	APS 24-ID-C	CHESS F1	CHESS F1
wavelength (Å)	0.9792	0.9792	0.9177	0.9177
Space group	*R*3	*R*3	*R*3	*R*3
a (Å)	110.9	110.6	110.9	111.2
c (Å)	58.3	58.1	55.7	57.1
Resolution, highest shell (Å)	1.76–1.70	1.39–1.34	1.86–1.80	1.55–1.50
No. of reflections used	136,728	269,001	92,848	278,660
No. of unique reflections	58,443; 29,111[a]	59,565	23,624	41,996
Redundancy	4.7 (4.6[b])	4.5 (3.8)	3.9 (3.7)	6.6 (5.9)
Completeness (%)	99.9 (100.0)	99.9 (99.9)	99.6 (100.0)	99.6 (100.0)
$\langle I \rangle / \langle \sigma_I \rangle$[c]	19.6 (3.2)	29.2 (2.9)	17.3 (2.0)	24.7 (1.7)
R_{merge} (%)[d]	7.0 (41.7)	4.3 (41.6)	5.4 (37.1)	5.3 (53.1)

[a] No. of Bijvoet pairs.

[b] Values in parentheses correspond to the highest resolution shell.

[c] <> indicates mean; *I* denotes intensity, and σI represents standard deviation of *I*.

[d] $R_{merge} = \sum_{i=1}^{N_U} \sum_{j=1}^{N_i} \left| I_j - \langle I \rangle_i \right| / \sum_{i=1}^{N_U} \sum_{j=1}^{N_i} I_j$, where N_U is the total number of unique reflections and N_i is the number of reflections measured for a given $i = hkl$.

TABLE 2

Refinement Statistics.

	SeMet-TflA	Apo-TflA	Holo-TflA	TflA-Tox-Mn
No. of reflections	28,975	57,477	22,470	38,786
No. of reflections in working set	27,529	54,657	21,350	36,893
Resolution (Å)	1.70	1.34	1.80	1.50
No. of protein atoms	1,733	1,772	1,725	1,733
No. of waters	224	253	147	187
No. of ligand atoms	0	0	0	14
No. of metal ions	0	0	1	1
RMSD from ideal bonds (Å)	0.006	0.006	0.007	0.006
RMSD from ideal angles (deg)	1.067	1.085	1.079	1.032
R_{work} (%)[a]	17.4	17.2	18.9	20.6
R_{free} (%)[a]	19.4	18.5	22.3	23.0
Ramachandran analysis[b]				
Most favored (%)	91.3	91.3	89.2	90.2
Additional allowed (%)	8.2	8.2	10.3	9.3
Generously allowed (%)	0.0	0.0	0.0	0.0
Disallowed (%)	0.5	0.5	0.5	0.5

[a] $R_{work} = \sum_{i=1}^{N_U} \left| |F_{O,i}| - k|F_{C,i}| \right| / \sum_{i=1}^{N_U} |F_{O,i}|$, where $|F_{O,i}|$ and $|F_{C,i}|$ are the observed and calculated structure factor amplitudes for reflection $i = hkl$ and N_U is the number of unique reflections in the working set. For R_{free}, these sums were taken over a 5% subset of the reflections excluded during structure refinement.

[b] Excludes glycine, proline, and end residues.